Tree stem diameter estimation using inexpensive UAV photogrammetric data and Monte Carlo methods

Borja García-Pascual[1,2], Carlos Martín-Cortés[1,3], Xin Zhou[1], Evgeny Lopatin[4], Mauricio Acuna[2], Kalle Kärhä[1]

[1]School of Forest Sciences, University of Eastern Finland, 80101 Joensuu, Finland
[2]Forest technology and wood material solutions, Natural Resources Institute Finland (Luke), 80100 Joensuu, Finland
[3]Joint Research Unit (JRU) CTFC - AGROTECNIO, 25280 Solsona, Spain
[4]Bioeconomy policies and markets, Natural Resources Institute Finland (Luke), 80100 Joensuu, Finland

Keywords: Stem characterization, Photogrammetry, Structure from Motion, Diameter estimation, Unmanned aerial vehicle.

Abstract

Accurate diameter estimation from point cloud data allows for characterizing stem volume and shape without resorting to destructive methods. Typically, circles are fitted at various stem heights using statistical techniques. However, these techniques are susceptible to noise and occlusion in the point cloud, often caused by obstacles or weather phenomena. This susceptibility reduces the feasibility of applying such methods to point clouds captured by low-cost sensors, which tend to be less precise and noisier. Photogrammetry, however, can be used together with consumer-grade cameras and inexpensive UAVs to generate high-quality point clouds from under-canopy data.

This study presents MACiF (Morphology-Aware Circle Fit), a novel method to accurately estimate diameters at various heights from noisy point clouds. Our approach uses robust statistical methods and Monte Carlo simulation to filter the point cloud. We also leverage how stems vary gradually to iteratively correct erroneous estimates. This iterative correction enables estimating diameters with an error lower than -3.34 cm, even when data quality limits the use of other methods. These results support the use of under-canopy low-cost photogrammetry as a viable source of data for automatic stem characterization.

1. Introduction

Effective forest resource management is essential for enhancing carbon sequestration and securing a stable wood supply (Daigneault et al., 2022; Barrette et al., 2023). Forest inventorying serves as a fundamental component of sustainable forest management by providing critical data for planning and decision-making (Coops et al., 2023). Inventorying is typically conducted at multiple spatial scales, including forest- and tree-level assessments. Forest-scale surveys can assess the distribution, area, species composition and health status of regional forest resources, supporting management decisions and policymaking at the macro level (McCullagh et al., 2017). Tree-level inventories focus on capturing detailed structural and morphological attributes of individual trees, enabling accurate estimation of timber volume, biomass, and carbon storage, and facilitating precise forest management (Yin and Wang, 2016).

Advances in remote sensing technology have revolutionized forest resources characterization by generating detailed 3D models, typically in the form of point clouds (Murtiyoso et al., 2024). The use of point clouds has created new opportunities for forest inventorying without the need for manual measurements (Liang et al., 2016). These inventories typically involve detecting trees within the point cloud and fitting circles along each tree stem. This process allows not only volume estimation but also analysis of stem shape and taper equations (Prendes et al., 2023; Nurunnabi et al., 2024). For instance, Prendes et al. (2023) used 3D data to estimate stem curvature for optimizing log cutting.

Such 3D data can be generated by using active sensors such as LiDAR (Light Detection and Ranging) scanners. By emitting laser pulses and capturing reflections, LiDAR generates precise 3D point clouds while partially penetrating through canopy (Jia et al., 2021). Terrestrial laser scanning (TLS) offers the best results in terms of noisiness, but TLS sensors must remain static when scanning, impeding their use for large-scale inventorying (Bauwens et al., 2016). On the contrary, mobile laser scanners (MLS) enable scanning larger areas quickly as they are not fixed systems (Lin et al., 2022). However, MLS sensors generally produce noisier and less accurate point clouds (Bienert et al., 2018). Point clouds can also be generated using data acquired by passive sensors such as optical cameras. Although cameras are designed to obtain high-resolution 2D images, they can be employed to create detailed 3D models through photogrammetric techniques (Bonneval, 1972). Among these techniques, Structure from Motion (SfM) generates dense point clouds by tracking the location of objects in images acquired from different view-points (Ullman, 1979). This technique generates high-quality point clouds provided enough images and with sufficient resolution are used (Acuna and Sosa, 2019).

Optical and MLS sensors can be carried by foot to acquire data under canopy, but they can also be installed on unmanned aerial vehicles (UAVs). Deploying UAVs is efficient as they can navigate autonomously once a route is scheduled, covering wide areas in a much lower time than ground-based, human operated systems (Hyyppä et al., 2020b). Because cameras are more energy-efficient than laser sensors, they are better suited to be installed on UAVs (Reddy Cenkeramaddi et al., 2020). Moreover, cameras installed on aerial drones can be used along SfM algorithms to generate point clouds with comparable quality to laser systems (Acuna and Sosa, 2019).

This contribution has been peer-reviewed. The double-blind peer-review was conducted on the basis of the full paper.
https://doi.org/10.5194/isprs-annals-X-2-W2-2025-49-2025 | © Author(s) 2025. CC BY 4.0 License.

In SfM-based forest inventorying applications, UAVs are generally used above canopy given forests are complex and obstacle-rich environments. Such setups typically yield poor data on tree stems, as canopy occludes most under-canopy information (Hyyppä et al., 2020b). However, UAVs can also be deployed under canopy equipped with optical and depth sensors for SfM-based inventorying (Karjalainen et al., 2025). Provided they are integrated with obstacle detection algorithms, UAVs can move through forests autonomously while avoiding obstacles, as shown by Karjalainen et al. (2025). Nonetheless, branches, undergrowth, and weather conditions can introduce noise or partially occlude trunks (Wilkes et al., 2017). Thus, diameter estimation methods robust to noise and occlusion are needed.

Several methods allow to estimate diameters from stem point clouds. The simplest approach to estimate diameters is least squares (LS) optimization, as used by Henning & Radtke (2006). This method reduces the algebraic distance of each point to the fitted circle through non-linear least squares optimisation. Alternatively, the geometric distance can be used as the objective function for an optimisation problem. In that case, steepest descent algorithms can be employed to fit the optimal circle, yielding higher precision than regular LS algorithms (Koreň et al., 2017). Hough Transform (HT) can be used to fit circles to point clouds (Hough, 1962), although it is computationally expensive. To deal with this limitation, Trochta et al. (2017) used Randomised Hough Transform (RHT) to speed the circle fitting process. Since these methods are sensitive to noise, Nurunnabi et al. (2024) used Monte Carlo simulation to generate candidate circles ignoring half the points. These circles are then ranked by their residual with respect to the points used and the best one is returned. To deal with noise, 3DFin software (Laino et al., 2024) uses LS for an initial circle fit and checks its quality; they check whether there are parts of perimeter without nearby points and if there are points inside the circle. In case the circle is considered deficient, DBSCAN filtering is applied iteratively to remove noise.

Even if some of the methods listed above integrate noise-filtering mechanisms, they often produce inaccurate estimates in poor-quality stem sections. However, it can be safely assumed that accurate estimates in one section may help correct neighbouring ones, as stem shape and diameter change gradually with height. Given a sufficiently small distance between adjacent sections, diameters and circle centres should be similar. Therefore, we present Morphology-Aware Circle Fit (MACiF), an algorithm to correct erroneous predictions based on the natural morphology of stems.

2. Objectives

The main objective of this study is to develop and validate a new circle-fitting algorithm capable of correcting inaccurate estimates using data from adjacent stem sections. We also aim at providing insights into how inexpensive photogrammetric point cloud modelling can be a viable alternative to LiDAR scanning. Lastly, we intend to underscore the limitations of current diameter estimation algorithms, and the methods used to validate them. The specific objectives of our work are:

1. Simulate high-density noise to test the limits of current diameter estimation methods.
2. Integrate the stem shape continuity hypothesis to correct estimation errors in low-quality sections.
3. Evaluate the accuracy and robustness of the proposed method compared to previous approaches under varying levels of noise.

3. Materials and methods

In the present study we followed a series of steps to validate the robustness of our method. Firstly, we measured diameter at breast height (DBH) of 18 trees within a 10 m radius plot, all pertaining to the same species. We then flew a drone under canopy to collect images where stems were clearly visible. These images served to reconstruct a point cloud, from which stems were later segmented and modified to simulate branches. These point clouds were used to estimate DBH, and results were compared to manual measurements (Figure 1).

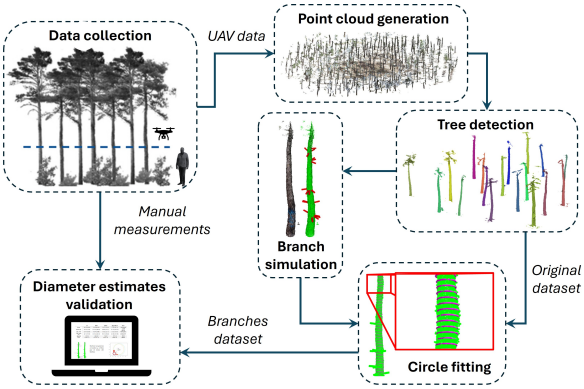

Figure 1. Overview of the workflow followed in this study.

3.1 Data collection

For this study, field data collection was divided into three phases: study area definition, manual marking and measuring of trees, and UAV data collection. Data collection was conducted approximately 3 km east of Hernansancho, in the province of Ávila (see Figure 2). A 20-meter measuring tape was employed to define a circular plot with 10 m radius, resulting in a total area of approximately 314 m^2. The plot was located in an even-aged homogeneous forest stand of adult *Pinus pinaster* Aiton managed for resin production. This stand has been previously subjected to thinning operations and presented a density of 513 trees per hectare.

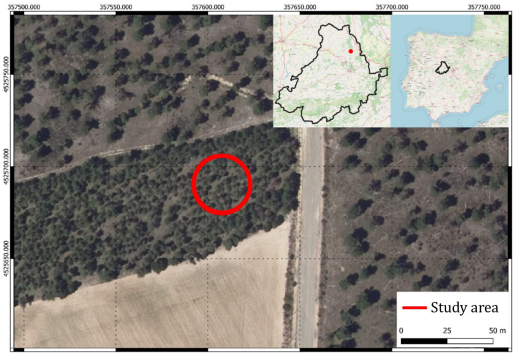

Figure 2. Orthoimage of the study area.

Within the study area, 18 specimens of *P. pinaster* were marked, and their diameter at breast height (DBH) was measured. To do so, we used tape with an accuracy of 0.1 cm to measure stem perimeter at 1.30 m height, after which we computed its equivalent circle diameter as follows:

$$d = \frac{p}{\pi}, \qquad (1)$$

where p = circle perimeter

Aerial imagery was captured using a DJI Mini 2 quadcopter (DJI, Shenzhen, China), a compact UAV (Unmanned Aerial Vehicle) with a take-off weight of 249 g and a retail price below €500 (initial European market price). The drone features a 1/2.3" CMOS sensor capable of capturing 12 MP images. A single flight was conducted under canopy conditions at an average altitude of approximately 1.5 meters above the ground. The environment had minimal low vegetation, making it feasible and safe to operate the drone beneath the canopy. Images were taken every 2 seconds along the tree planting lines. The flight below canopy was performed manually, avoiding obstacles and trees in the study area. Figure 3 shows the route taken to collect data and the location of the inventoried trees. The flights took place around 10:00 AM under sunny, windless conditions. A total of 394 images were collected during a 13.3-minutes flight. The route followed was devised so that all stems where visible from all sides.

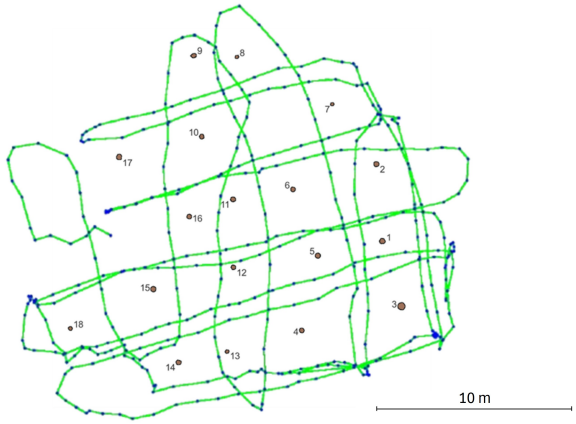

Figure 3. Path followed by the UAV during data acquisition (green), points from which pictures were taken (blue) and location of the trees (brown).

3.2 Photogrammetric data processing

To process UAV data, we used Pix4Denterprise version 4.5.6 (Pix4D, 2020). This process was performed on a consumer-grade MSI GL62M 7RD-056 (MSI) computer equipped with an Intel® Core™ i7-7700HQ CPU @ 2.80 GHz, 16 GB of RAM, and an NVIDIA GeForce® GTX1050 GPU, operating on Windows 10 Pro 64-bit. For dense point cloud generation, a 1/2 image scale setting with optimal point density was selected. This process yielded a point cloud comprised of 6,939,608 3D points, corresponding to an average point density of 7,642.53 points per cubic meter. The result of this photogrammetric processing can be seen in Figure 4.

Figure 4. Dense point cloud obtained from SfM reconstruction.

3.3 Photogrammetric data processing

Once the dense point cloud was generated, we manually cropped the region of interest containing the manually measured trees. This cropped region was segmented using the Python package 3DFin (Laino et al., 2024). This software first detected ground points resorting to the cloth simulation filter (CSF) algorithm (Zhang et al., 2016) with a height threshold of 0.1 m. The ground served to normalize the point cloud, from which a 2 m wide stripe was extracted to detect and individualize tree stems (Figure 5). The validity of the resulting stem detection was visually inspected using the open-source CloudCompare software (Girardeau-Montaut, 2024). We then aligned each tree stem along the vertical Z-axis using principal Component Analysis (PCA), standardizing point cloud orientation.

Figure 5. Individual trees detected and coloured by instance.

After inspecting the resulting point clouds, we noted stems were lacking noise from branches or understory. Such noise is expected to have little impact on our algorithm, as it uses good quality sections of the stem to correct wrong predictions. Noise can also be ignored by HyperRLTS, as it discards 50% of the points when fitting circles. Nonetheless, if noise-to-signal ratio is large enough, such mechanism might be rendered insufficient. Therefore, we simulated branches by generating high-density noise uniformly along lines of random length and orientation. To do so, we used circles fitted on the original stems through least squares to estimate where their surface was. Because the original stem point clouds had little noise, these circles adjusted tight enough to the real stem surface. Sprouting from circles' perimeter, between one and six branches were generated at different stem heights; branches were always generated at 1.3 m height to assess their effect on DBH estimation. These branches had a length ranging from 0.15 m to 1 m, along which points were randomly scattered. Point-to-branch distance, however, never exceeded 2 cm to prevent excessive noise. As a result, two different datasets were used in the present study: *original* and *branches* (Figure 6).

Figure 6. Original point cloud (left) and point cloud with simulated branches. Stem points are depicted in green; branches are depicted in red (right).

For each of the trees comprising both datasets, a 7 cm thick section centred at 1.30 m was extracted and projected onto the XY plane. These projected points served to fit circles and estimate the trunk's centre and diameter using different circle fitting methods. To characterize the full stem, the cloud was divided into 7 cm thick slices with a step size of 3.5 cm, producing a detailed stem profile.

This contribution has been peer-reviewed. The double-blind peer-review was conducted on the basis of the full paper.
https://doi.org/10.5194/isprs-annals-X-2-W2-2025-49-2025 | © Author(s) 2025. CC BY 4.0 License.

3.4 Morphology-Aware Circle Fit (MACiF)

Our method, MACiF, builds on the circle fitting algorithm HyperRLTS, which was developed by Nurunnabi et al. (2024). HyperRLTS defines a circle by randomly selecting three points from a 2D-projected slice, running the process 69 times as per Nurunnabi et al. (2015). For each candidate circle, the distance of all points in the cloud to its perimeter are calculated and ranked in descending order. The 50% of points closest to the perimeter are then used to fit a refined new circle using the Hyper method (Kanatani and Rangarajan, 2011). Among the 69 refined circles fitted, the one with the lowest mean squared error (MSE) is returned.

MACiF uses HyperRLTS as baseline to fit initial circles along the stem, which are then corrected based on stem's shape. To correct circles, we integrated an iterative correction module based on the assumption that stems change gradually both in diameter size and core location (Figure 7). The iterative correction module first runs a sliding window algorithm to extract 7 cm-thick slices along the stem as described in the preprocessing step. Each slice was then used to fit a circle by employing HyperRLTS. Next, sections and their corresponding fitted circles were grouped using a sliding window of 10 sections. The 10-sections window was then moved along the entire stem with a step size of one section. Among all the 10-sections groups, the one with the least variability was assumed to be of higher quality.

Variability was assessed using three linear regression models, one for each of the dependent variables used: fitted circle's centroid X-coordinate, Y-coordinate, and radius. These regression models were adjusted from the circles fitted across the entire stem using height as independent variable. For each 10-sections group, the regression models were applied to predict circles' centroid coordinates and radius from section height. These group predictions were then used to compute the relative mean squared error and averaged as follows:

$$RelMSE = \frac{1}{M}\sum_{m=1}^{M}\sum_{n=1}^{N}\frac{\left(y_{m,n}-\hat{y}_{m,n}\right)^2}{\left(y_{m,n}-\bar{y}_m\right)^2}, \qquad (2)$$

where M = number of models use
N = number of samples
m = index of the variable predicted by each model
$y_{m,n}$ = ground truth value for variable m and sample n
$\hat{y}_{m,n}$ = value of value m predicted by the regression model for sample n
$\bar{y}_m$ = average ground truth value for variable m

In turn, the relative mean squared error of a group measures its deviation from a perfectly straight stem with diameters changing linearly with height. Therefore, the group that scores the best is the one closest to a perfect stem; such section group was regarded as the reference group, which served to correct all fitted circles along the stem. To avoid including outliers in the reference group, the robust Z-value (Rz) for each circle's X and Y coordinates, and circle radius was computed as described in Nurunnabi et al. (2015). Anomalous values (Rz > 2.5) were replaced by linear interpolation, and the resulting 10-section group became the reference.

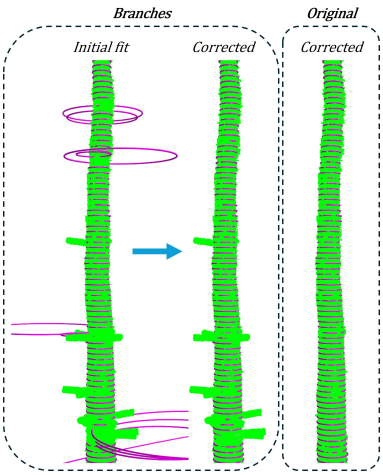

Figure 7. Fitted circles fitted before correction on a *branches* dataset sample and its corrected version next to it (left side); corrected version of the same sample before branch simulation (right side). Fitted circles are depicted in magenta.

Once we identified the reference group, the overlap between its last fitted circle and the immediately adjacent non-reference one was evaluated using the Jaccard's index (1901), referred to as IoU hereafter:

$$IoU_{RA} = \frac{S_R \cap S_A}{S_R \cup S_A}, \qquad (3)$$

where S_R = surface of the last reference circle
S_A = surface of the adjacent circle

If the IoU_{RA} was greater or equal than 0.75, the adjacent circle was considered as correct and added to the reference group. Otherwise, the 2D-projected section used to fit the adjacent circle was cropped using the last reference circle as kernel. Three cropping radii were tested, each radius spanning between 1.1 and 1.5 times the radius of the last reference circle. Section cropping was done as part of a Monte Carlo simulation process, in which newly cropped sections were fit a circle using HyperRLTS. The resulting fitted circles were ranked by their MSE and their IoU_{RA} with respect to the reference circle were computed. Among the five fitted circles with the least MSE, the one with the highest IoU_{RA} was added to the reference group.

3.5 Method validation

To validate the performance of our algorithm, we applied four other circle fitting methods to estimate DBH on both datasets, *original* and *branches*. These estimates were then compared to manually measured diameters at breast height. We applied least squares (LS), random hough transform (RHT) (Trochta et al., 2017), 3DFin (Laino et al., 2024), and HyperRLTS (Nurunnabi et al., 2024). It must be noted that 3DFin can assess circle fit quality based on the number of points within the circle and along its perimeter. In this comparison, however, all predictions were included regardless of their quality.

4. Results

When evaluated on the *original* dataset, all the tested methods performed similarly, presenting a tendency towards underestimation (see Table 1). RHT yielded the highest average error (-3.78 cm) and absolute error (4.06 cm), although standard deviation was the lowest. On the contrary, our method provided

the best DBH estimates across all metrics, only bested by HyperRLTS when comparing least squared error. All in all, differences were small; error ranged from -14.50% (RHT) to -12.48% (Ours), and absolute error ranged from 15.50% (RHT) to 14.87% (Ours).

	Error		*Abs. error*		*Squared error*
	cm	%	cm	%	
LSQ	-3.43 (3.53)	-12.92 (10.44)	4.01 (2.84)	14.97 (**7.20**)	24.17 (45.99)
RHT	-3.78 (**3.25**)	-14.50 (**9.55**)	4.06 (2.89)	15.50 (7.82)	24.84 (46.81)
3DFin	-3.43 (3.53)	-12.92 (10.44)	4.01 (2.84)	14.97 (**7.20**)	24.17 (45.99)
HyperRLTS	-3.38 (3.53)	-12.85 (10.69)	4.01 (**2.79**)	15.04 (7.28)	**23.83** (**44.12**)
MACiF	**-3.31** (3.70)	**-12.48** (11.29)	**4.00** (2.94)	**14.87** (7.89)	24.64 (45.26)

Table 1. Average error (cm), absolute error (cm), and mean squared error (cm²) for DBH estimation methods tested on the *original* dataset; standard deviation in parentheses.

Point clouds in the *branches* dataset resulted on average 3.89 times denser than in the *original* dataset. Because branches were simulated in variable numbers and with length and girth, point cloud size in the *branches* dataset ranged from 1.91 to 5.46 times the size of their corresponding *original* sample. When evaluated on the *branches* dataset, MACiF outperformed all other methods in every metric (Table 2). Furthermore, our algorithm performed similarly on both *original* and *branches* datasets; in the latter, the unsigned average error was only 0.06 cm greater than in the former, whereas the absolute error increase only by 0.02 cm. Standard deviation was also similar to the *original* case, hence suggesting low variance in the DBH estimation error. Notably, after applying our iterative correction algorithm the HyperRLTS baseline improved considerably; the average relative error reduced from 217.54% to -12.98%.

	Error		*Abs. error*		*Squared error*
	cm	%	cm	%	
LSQ	10.59 (16.60)	42.39 (57.69)	11.47 (16.00)	44.72 (55.90)	387.61 (1302.57)
RHT	31.00 (60.85)	135.38 (289.94)	34.59 (58.88)	147.04 (284.20)	4663.82 (15123.75)
3DFin	14.57 (23.93)	64.69 (112.21)	16.32 (22.77)	69.33 (109.40)	784.99 (1974.76)
HyperRLTS	51.50 (56.73)	217.54 (239.12)	53.32 (55.03)	223.08 (233.96)	5871.30 (9460.18)
MACiF	**-3.37** (**3.46**)	**-12.79** (**10.36**)	**4.02** (**2.68**)	**15.05** (**6.67**)	**23.34** (**41.89**)

Table 2. Average error (cm), absolute error (cm), and mean squared error (cm²) for DBH estimation methods tested on the *branches* dataset; standard deviation in parentheses.

Although centroid deviation from the trunk axis remained unquantified, results were visually evaluated. Figure 8 shows that our method aligned well with true stem positions, even when branches were included, while other methods suffered from interference. Circle fitting along the stem was also visually assessed. MACiF yielded good results along stems on both datasets, including curved and crooked stems. Nonetheless, we noted errors increased at the upper parts of the stem, as severe occlusion and point cloud sparsity prevented reliable correction in these areas.

5. Discussion

5.1 UAV photogrammetry for forest inventorying

The results of this study are consistent with those of previous research on SfM-based diameter estimation (Krisanski et al., 2020; Shimabuku et al., 2023; Karjalainen et al., 2025). These results underscore the potential of UAV-based photogrammetry as a viable low-cost alternative to laser technologies for generating detailed three-dimensional models of forests. Furthermore, they stress the potential of under-canopy UAV data acquisition, as above-canopy UAV laser scanning data typically exhibits lower surface density and noisier point clouds compared to terrestrial data (Kuželka et al., 2020). Above-canopy laser-based trunk detection methods are also susceptible to noise, occlusion, presence of branches and ground vegetation, cross-section scattering, and uneven point densities (Kuželka et al., 2020; Dersch et al., 2021). For instance, Zhang et al. (2023) demonstrated that understory vegetation and branches can be erroneously identified as tree trunks, leading to over-detection. On the contrary, under-canopy data provides a high-quality description of tree stems (Hyyppä et al., 2020b).

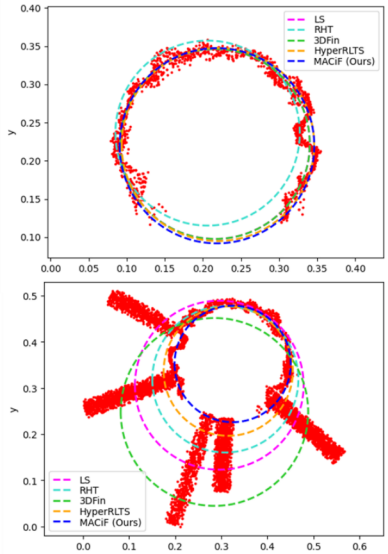

Figure 8. Circle fitting using different methods on the *original* (top row) and on the *branches* (bottom row) datasets; *X* and *Y* coordinates displayed in meters.

Other ground-based low-cost technologies such as modern LiDAR-enabled smart devices can serve to estimate tree diameter. Nonetheless, they are limited in range and so their use is restricted to small plots were only data from the lower parts of the stems is needed (Tatsumi et al., 2023). Moreover, using UAV drones presents distinct advantages over such technologies. Because they hover over understory, they are unaffected by rugged terrain or low shrubs, covering large areas efficiently (Hyyppä et al., 2020b). In addition, they typically integrate gimbal stabilizers to ensure steady image acquisition. Lastly, they can fly autonomously if they integrate proper perception and navigation systems, and the right forest conditions are given (Karjalainen et al., 2025). In contrast to ground-based robots, drones offer agility and versatility in data acquisition, although they remain hindered by understory vegetation density (Hyyppä et al., 2020a).

Many lightweight UAV models are more affordable than modern LiDAR-equipped smart devices. Furthermore, drones weighing under 250 grams benefit from more flexible regulatory frameworks (European Union Aviation Safety Agency, 2024), potentially simplifying their deployment for automated forest monitoring systems. Open-source photogrammetry tools further lower barriers by eliminating costly software licenses, making them economically viable for forestry applications. To fully integrate these technologies into forest planning and decision-making processes, however, more

efficient algorithms capable of handling large data volumes are needed. Such algorithms must also be capable of accurately reconstructing large, complex, and dynamic scenes. Crucially, recent advances in three-dimensional modelling from images are bridging this gap: neural-based rendering and Gaussian splatting have reduced computation time required to obtain 3D models (Mildenhall et al., 2021; Kerbl et al., 2023), while improving model quality.

5.2 Circle fitting evaluation

Error in DBH estimation when using the *original*, clean dataset was consistent among all methods and never exceeded 4 cm in absolute terms. This consistency is likely because photogrammetric point clouds presented little noise on the stem surface. Despite all methods yielding similar results, our method outperformed all the others, including HyperRLTS. HyperRLTS was used by MACiF to fit initial circles, which were corrected only when they were deficient. Given *original* dataset's quality, the correction module remained unused, hence differences with HyperRLTS were small and possibly caused by its randomized nature. We also found error to be consistently caused by diameter underestimation, averaging close to -3 cm for all methods. A plausible explanation for this bias is the natural morphology of *P. pinaster*, which normally grows thick, rugged bark with deep, longitudinal cracks (Blanco Castro, 2005). Bark plates' crests cause manual measurement to overestimate the stem diameter, hence the negatively signed error of circles fitted to crack valleys. This phenomenon underscores the importance of validating MACiF on a dataset comprised of several tree species, which will be accounted for in future studies.

On the contrary, when evaluated on the *branches* dataset, MACiF outcompeted all other methods, including HyperRLTS. Under such conditions, simulated noise caused previous methods to fail, hence MACiF's initial fit required correction. The iterative correction module then allowed removing enough noise so that HyperRLTS dealt with remaining noise effectively. This claim is supported by MACiF results differing little between the *original* and the *branches* dataset; in fact, such difference is small enough to be considered as an effect of algorithmic randomisation. Both numerical results and visual assessment support the claim that iterative correction based on stem continuity improves diameter estimation accuracy. Furthermore, visual inspection of MACiF's predictions along stems indicates it has potential for tree structure modelling; our method accounts for natural stems' morphology, hence yielding accurate stem shape models. Although, forked stems pose an important challenge, as MACiF is compelled to follow either of the branches when correcting predictions.

In the light of these results, we hypothesize MACiF only requires a good reference section group and enough signal points along stems' surface to perform well. However, the effect of random noise and occlusion on our algorithm remains untested: if the reference group includes failed fits or later corrections fail due to random noise or occlusion, errors may propagate. Besides, MACiF could also benefit from other noise filtering techniques. For example, 3DFin uses DBSCAN for noise removal and evaluates circle fit quality via point density. Therefore, future versions of our algorithm will test integrating such enhancements.

Yet, the main limitation of this study is the lack of data. We only used a sample of 18 trees, from which we obtained point clouds using a single 3D modelling technique; MACiF should be tested on LiDAR data, as point distribution and density can vary greatly with respect to SfM point clouds. Furthermore, we lack tree diameter measurements above and below 1.3 m, which is crucial to validate the robustness of our method when applied along the stem. We also stress a key limitation of studies assessing stem diameters using point clouds: stem core location is rarely accounted for. In some cases, circle fitting methods yield good results in terms of diameter estimation, yet circle centroid location is displaced. Centroid location is crucial for applications such as optimal bucking (Prendes et al., 2023), hence the need for better circle fitting validation strategies. Last, we also note that circle fitting methods do not account for the actual shape of stem cross-sections, ignoring the natural complexity of tree stems and incurring in estimation errors (Kuželka and Surový, 2024). Cross-sectional stem shape is important for timber market value assessment, as it is often assessed using gauging methods such as Japanese Agricultural Standard (JAS) (Ellis et al., 1996).

As for data scarcity, a possible solution is using simulation methods. In the present study, we used a simple, yet effective strategy to assess the impact of high-density noise on circle fitting methods by generating branches. Other noise generation strategies might enable testing circle fitting methods on point clouds with greater point dispersion and random noise (Nurunnabi et al., 2015). More sophisticated methods, nonetheless, allow generating realistic tree point clouds for which diameter at different heights and stem core locations would be perfectly known (Bornand et al., 2024). Therefore, future research will focus on testing the robustness of different circle fitting methods to various degrees of noise using complex three-dimensional tree modelling.

6. Conclusion

In this study we developed and evaluated MACiF (Morphology-Aware Circle Fit), a new algorithm for estimating stem diameters from point clouds. The method integrates robust statistical fitting with an iterative correction process that leverages stem shape continuity. This approach significantly improves accuracy in noisy or occluded point clouds, outperforming existing methods in both clean and simulated-noise scenarios. Our results demonstrate that low-cost UAV photogrammetry, when combined with morphology-aware processing, can provide reliable stem measurements for forest inventory applications.

Despite these promising results, several limitations remain. Validation was limited to 18 trees and to diameter at breast height; further testing on larger datasets acquired with different sensors, other stem heights, and from tree species is needed. Additionally, incorporating advanced noise filtering techniques could further enhance robustness. Notwithstanding, MACiF represents a step forward in precise tree diameter and stem shape estimation, contributing to the broader goal of Forestry 4.0.

7. Acknowledgments

The authors gratefully acknowledge partial funding from the Research Council of Finland and its Flagship program through the UNITE project. They also acknowledge partial funding from the European Union's Horizon Europe research and innovation programme under grant agreement No 101082051 through the SINTETIC project. The authors are also thankful to Juan Carlos Martín Pérez for his aid during the manual data collection campaign.

8. References

Acuna, M., Sosa, A., 2019. Automated Volumetric Measurements of Truckloads through Multi-View Photogrammetry and 3D Reconstruction Software. *Croat. J. For. Eng.* 40, 151–162.

Barrette, J., Achim, A., Auty, D., 2023. Impact of Intensive Forest Management Practices on Wood Quality from Conifers: Literature Review and Reflection on Future Challenges. *Curr. For. Rep.* 9, 101–130. https://doi.org/10.1007/s40725-023-00181-6

Bauwens, S., Bartholomeus, H., Calders, K., Lejeune, P., 2016. Forest Inventory with Terrestrial LiDAR: A Comparison of Static and Hand-Held Mobile Laser Scanning. *Forests* 7, 127. https://doi.org/10.3390/f7060127

Bienert, A., Georgi, L., Kunz, M., Maas, H.-G., Von Oheimb, G., 2018. Comparison and Combination of Mobile and Terrestrial Laser Scanning for Natural Forest Inventories. *Forests* 9, 395. https://doi.org/10.3390/f9070395

Blanco Castro, E., 2005. *Los bosques ibéricos: una interpretación geobotánica*, 4th ed. Planeta, Barcelona.

Bonneval, H., 1972. *Photogrammétrie générale*. Eyrolles, Paris.

Bornand, A., Abegg, M., Morsdorf, F., Rehush, N., 2024. Completing 3D point clouds of individual trees using deep learning. *Methods. Ecol. Evol.* 15, 2010–2023. https://doi.org/10.1111/2041-210X.14412

Coops, N.C., Tompalski, P., Goodbody, T.R.H., Achim, A., Mulverhill, C., 2023. Framework for near real-time forest inventory using multi source remote sensing data. *Forestry* 96, 1–19. https://doi.org/10.1093/forestry/cpac015

Daigneault, A., Baker, J.S., Guo, J., Lauri, P., Favero, A., Forsell, N., Johnston, C., Ohrel, S.B., Sohngen, B., 2022. How the future of the global forest sink depends on timber demand, forest management, and carbon policies. *Glob. Environ. Change.* 76, 102582. https://doi.org/10.1016/j.gloenvcha.2022.102582

Dersch, S., Heurich, M., Krueger, N., Krzystek, P., 2021. Combining graph-cut clustering with object-based stem detection for tree segmentation in highly dense airborne lidar point clouds. *ISPRS J. Photogramm. Remote Sens.* 172, 207–222. https://doi.org/10.1016/j.isprsjprs.2020.11.016

Ellis, J.C., Sanders, D.H., Pont, D., 1996. JAS log volumes estimates of New Zealand radiata pine and Douglas-fir logs. *N. Z. Forestry* 41, 32–36.

European Union Aviation Safety Agency, 2024. Open Category — Low Risk — Civil Drones [WWW Document]. *EASA*. URL https://www.easa.europa.eu/en/domains/drones-air-mobility/operating-drone/open-category-low-risk-civil-drones (accessed 4.17.25).

Girardeau-Montaut, D., 2024. CloudCompare Software, Version 2.13.1. CloudCompare Open Source Project. cloudcompare.org (20 March 2024).

Henning, J.G., Radtke, P.J., 2006. Detailed Stem Measurements of Standing Trees from Ground-Based Scanning Lidar. *For. Sci.* 52, 67–80. https://doi.org/10.1093/forestscience/52.1.67

Hough, P.V.C., 1962. Method and means for recognizing complex patterns. US3069654A.

Hyyppä, E., Hyyppä, J., Hakala, T., Kukko, A., Wulder, M.A., White, J.C., Pyörälä, J., Yu, X., Wang, Y., Virtanen, J.-P., Pohjavirta, O., Liang, X., Holopainen, M., Kaartinen, H., 2020a. Under-canopy UAV laser scanning for accurate forest field measurements. *ISPRS J. Photogramm. Remote Sens.* 164, 41–60. https://doi.org/10.1016/j.isprsjprs.2020.03.021

Hyyppä, E., Yu, X., Kaartinen, H., Hakala, T., Kukko, A., Vastaranta, M., Hyyppä, J., 2020b. Comparison of Backpack, Handheld, Under-Canopy UAV, and Above-Canopy UAV Laser Scanning for Field Reference Data Collection in Boreal Forests. *Remote Sens.* 12, 3327. https://doi.org/10.3390/rs12203327

Jaccard, P., 1901. Étude comparative de la distribution florale dans une portion des Alpes et des Jura. *Bull. Soc. Vaudoise. Sci. Nat.* 37, 547–579.

Jia, J., Sun, H., Jiang, C., Karila, K., Karjalainen, M., Ahokas, E., Khoramshahi, E., Hu, P., Chen, C., Xue, T., Wang, T., Chen, Y., Hyyppä, J., 2021. Review on Active and Passive Remote Sensing Techniques for Road Extraction. *Remote Sens.* 13, 4235. https://doi.org/10.3390/rs13214235

Kanatani, K., Rangarajan, P., 2011. Hyper least squares fitting of circles and ellipses. *Comput. Stat. Data Anal.* 55, 2197–2208. https://doi.org/10.1016/j.csda.2010.12.012

Karjalainen, V., Koivumäki, N., Hakala, T., Muhojoki, J., Hyyppä, E., George, A., Suomalainen, J., Honkavaara, E., 2025. Towards autonomous photogrammetric forest inventory using a lightweight under-canopy robotic drone. https://doi.org/10.48550/arXiv.2501.12073

Kerbl, B., Kopanas, G., Leimkühler, T., Drettakis, G., 2023. 3D Gaussian Splatting for Real-Time Radiance Field Rendering. https://doi.org/10.48550/arXiv.2308.04079

Koreň, M., Mokroš, M., Bucha, T., 2017. Accuracy of tree diameter estimation from terrestrial laser scanning by circle-fitting methods. *Int. J. Appl. Earth Obs. Geoinf.* 63, 122–128. https://doi.org/10.1016/j.jag.2017.07.015

Krisanski, S., Taskhiri, M., Turner, P., 2020. Enhancing Methods for Under-Canopy Unmanned Aircraft System Based Photogrammetry in Complex Forests for Tree Diameter Measurement. *Remote Sens.* 12, 1652. https://doi.org/10.3390/rs12101652

Kuželka, K., Slavík, M., Surový, P., 2020. Very High Density Point Clouds from UAV Laser Scanning for Automatic Tree

Stem Detection and Direct Diameter Measurement. *Remote Sens.* 12, 1236. https://doi.org/10.3390/rs12081236

Kuželka, K., Surový, P., 2024. Noise Analysis for Unbiased Tree Diameter Estimation from Personal Laser Scanning Data. *Remote Sens.* 16, 1261. https://doi.org/10.3390/rs16071261

Laino, D., Cabo, C., Prendes, C., Janvier, R., Ordonez, C., Nikonovas, T., Doerr, S., Santin, C., 2024. 3DFin: a software for automated 3D forest inventories from terrestrial point clouds. *Forestry* 97, 479–496. https://doi.org/10.1093/forestry/cpae020

Liang, X., Kankare, V., Hyyppä, J., Wang, Y., Kukko, A., Haggrén, H., Yu, X., Kaartinen, H., Jaakkola, A., Guan, F., Holopainen, M., Vastaranta, M., 2016. Terrestrial laser scanning in forest inventories. *ISPRS J. Photogramm. Remote Sens.* 115, 63–77. https://doi.org/10.1016/j.isprsjprs.2016.01.006

Lin, Y.-C., Shao, J., Shin, S.-Y., Saka, Z., Joseph, M., Manish, R., Fei, S., Habib, A., 2022. Comparative Analysis of Multi-Platform, Multi-Resolution, Multi-Temporal LiDAR Data for Forest Inventory. *Remote Sens.* 14, 649. https://doi.org/10.3390/rs14030649

McCullagh, A., Black, K., Nieuwenhuis, M., 2017. Evaluation of tree and stand-level growth models using national forest inventory data. *Eur. J. Forest. Res.* 136, 251–258. https://doi.org/10.1007/s10342-017-1025-8

Mildenhall, B., Srinivasan, P.P., Tancik, M., Barron, J.T., Ramamoorthi, R., Ng, R., 2021. NeRF: representing scenes as neural radiance fields for view synthesis. *Commun. ACM* 65, 99–106. https://doi.org/10.1145/3503250

Murtiyoso, A., Cabo, C., Singh, A., Obaya, D.P., Cherlet, W., Stoddart, J., Fol, C.R., Beloiu Schwenke, M., Rehush, N., Stereńczak, K., Calders, K., Griess, V.C., Mokroš, M., 2024. A Review of Software Solutions to Process Ground-based Point Clouds in Forest Applications. *Curr. For. Rep.* 10, 401–419. https://doi.org/10.1007/s40725-024-00228-2

Nurunnabi, A., West, G., Belton, D., 2015. Outlier detection and robust normal-curvature estimation in mobile laser scanning 3D point cloud data. *Pattern Recognit.* 48, 1404–1419. https://doi.org/10.1016/j.patcog.2014.10.014

Nurunnabi, A.A.M., Teferle, F., Novo, A., Balado, J., Ientilucci, E., 2024. Derivation of Tree Stem Curve and Volume Using Point Clouds, in: *ISPRS Archives*. Presented at the 19th 3D GeoInfo Conference 2024, 1–3 July 2024, Vigo, Spain, International Society for Photogrammetry and Remote Sensing. https://doi.org/10.5194/isprs-archives-XLVIII-4-W11-2024-81-2024

Pix4D, 2020. PIX4Denterprise Software, Version 4.5.6.

Prendes, C., Acuna, M., Canga, E., Ordoñez, C., Cabo, C., 2023. Optimal bucking of stems from terrestrial laser scanning data to maximize forest value. *Scand. J. For. Res.* 38, 174–188.

Reddy Cenkeramaddi, L., Bhatia, J., Jha, A., Kumar Vishkarma, S., Soumya, J., 2020. A Survey on Sensors for Autonomous Systems, in: *2020 15th ICIEA*. Presented at the 2020 15th ICIEA, pp. 1182–1187. https://doi.org/10.1109/ICIEA48937.2020.9248282

Shimabuku, F., Konoshima, M., Ota, I., 2023. Diameter and stem volume estimation based on under canopy UAV-SfM-MVS survey approach in subtropical forest of Okinawa Island, Japan. *FORMATH* 22. https://doi.org/10.15684/formath.22.004

Tatsumi, S., Yamaguchi, K., Furuya, N., 2023. ForestScanner: A mobile application for measuring and mapping trees with LiDAR-equipped iPhone and iPad. *Methods Ecol. Evol.* 14, 1603–1609. https://doi.org/10.1111/2041-210X.13900

Trochta, J., Krůček, M., Vrška, T., Král, K., 2017. 3D Forest: An application for descriptions of three-dimensional forest structures using terrestrial LiDAR. *PLOS ONE* 12, e0176871. https://doi.org/10.1371/journal.pone.0176871

Ullman, 1979. The interpretation of structure from motion. *Proc. R. Soc. Lond. B.* 203, 405–426. https://doi.org/10.1098/rspb.1979.0006

Wilkes, P., Lau, A., Disney, M., Calders, K., Burt, A., Gonzalez de Tanago, J., Bartholomeus, H., Brede, B., Herold, M., 2017. Data acquisition considerations for Terrestrial Laser Scanning of forest plots. *Remote Sens. Environ.* 196, 140–153. https://doi.org/10.1016/j.rse.2017.04.030

Yin, D., Wang, L., 2016. How to assess the accuracy of the individual tree-based forest inventory derived from remotely sensed data: a review. *Int. J. Remote Sens.* 37, 4521–4553. https://doi.org/10.1080/01431161.2016.1214302

Zhang, W., Qi, J., Wan, P., Wang, H., Xie, D., Wang, X., Yan, G., 2016. An Easy-to-Use Airborne LiDAR Data Filtering Method Based on Cloth Simulation. *Remote Sens.* 8, 501. https://doi.org/10.3390/rs8060501

Zhang, Y., Tan, Y., Onda, Y., Hashimoto, A., Gomi, T., Chiu, C., Inokoshi, S., 2023. A tree detection method based on trunk point cloud section in dense plantation forest using drone LiDAR data. *For. Ecosyst.* 10, 100088. https://doi.org/10.1016/j.fecs.2023.100088